One-nucleon-transfer reactions induced by ^{20}Ne at 500 and 600 MeV

S. Fortier and S. Gales
Institut de Physique Nucléaire, 91406 Orsay CEDEX, France

Sam M. Austin, W. Benenson, G. M. Crawley, C. Djalali,* J. S. Winfield, and G. Yoo
National Superconducting Cyclotron Laboratory and Department of Physics and Astronomy, Michigan State University, East Lansing, Michigan 48824

(Received 14 September 1989; revised manuscript received 20 November 1989)

The (^{20}Ne,^{19}Ne), (^{20}Ne,^{21}Ne), and (^{20}Ne,^{21}Na) reactions on ^{90}Zr and ^{208}Pb have been investigated at 500 and 600 MeV incident energies. Experimental spectra have been compared with predictions of distorted-wave Born approximation calculations. The different shapes observed for proton and neutron pickup spectra are explained quite well by the calculations. In particular, the broad peak observed at about 6.5 MeV in the (^{20}Ne,^{21}Ne) spectra is shown to originate from ejectile excitation in the $1d_{3/2}$, $1f_{7/2}$, and $2p_{3/2}$ orbitals. An important component of the (^{20}Ne,^{19}Ne) cross section is due to three-body processes, such as the elastic breakup of ^{20}Ne into ^{19}Ne and one neutron. In addition, bumps are observed at about 1.5 and 10 MeV excitation energy in ^{209}Pb and 2.5 and 14 MeV in ^{91}Zr. The low energy peaks are shown to originate mainly from neutron transfer to high spin orbitals, i.e., $1i_{11/2}$ and $1j_{15/2}$ in ^{209}Pb and $1g_{7/2}$ and $1h_{11/2}$ in ^{91}Zr. Because of the selectivity of the (^{20}Ne, ^{19}Ne) reaction for large angular momentum transfer, it is proposed that the structures observed at 14 MeV in ^{91}Zr and 10 MeV ^{209}Pb are due to a neutron transfer to high spin orbitals, such as $1i_{13/2}$ and $1k_{17/2}$ in ^{91}Zr and ^{209}Pb, respectively.

I. INTRODUCTION

During the past few years, information about deep hole states and high-lying single-particle states in several medium and heavy nuclei have been obtained by studying light-ion reactions such as (p,d), (^{3}He,α) and (α^3,He).[1] Due to the selectivity of these reactions for transferring large values of angular momentum, the transfer of nucleons into or the pickup of nucleons from high spin orbitals was observed as large resonancelike bumps at high excitation energy. Unfortunately these reactions have been plagued by the presence of substantial backgrounds which lie under the peaks of interest, and further progress with light projectiles will necessitate disentangling the spectra by coincidence experiments. However, it also appears useful to investigate the capabilities of high energy heavy-ion reactions for studying these states. In some cases heavy-ion reactions are even more selective in exciting high spin states, the peak-to-background ratios may be more favorable and the excitation cross section can be larger than in the corresponding light-ion one-nucleon-transfer reactions.

In this paper we report an investigation of one-nucleon-transfer reactions induced by ^{20}Ne ions on ^{90}Zr and ^{208}Pb. The experiment was performed at two incident energies, 500 and 600 MeV, in order to use the kinematic shifts to disentangle transfer reactions from three-body processes. Calculations with the exact finite range distorted-wave Born approximation (EFR-DWBA) method were also performed, and these results are compared with the data. The main features of the spectra observed in the pickup reactions and the low excitation energy part of the stripping spectra are qualitatively well reproduced by DWBA calculations which include the mutual excitation of the quasitarget and ejectile nuclei, as described in Sec. III. At an excitation energy close to that of the giant quadrupole resonance in the corresponding target nucleus, the ^{90}Zr(^{20}Ne,^{19}Ne) and ^{208}Pb(^{20}Ne,^{19}Ne) spectra are dominated by a few MeV wide structure superimposed on a large bump due to fragmentation processes. From the arguments presented in Sec. IV it is proposed that this structure probably originates from neutron transfer to high spin orbitals.

II. EXPERIMENTAL CONDITIONS AND RESULTS

One-nucleon-transfer spectra were obtained during an experiment primarily devoted to a search[2] for high energy structures in ^{20}Ne inelastic scattering on ^{208}Pb and ^{90}Zr. Only some characteristics relevant to the present data will be given here, as the details of this experiment have been reported previously.[2]

The measurements were carried out with 500 and 600 MeV ^{20}Ne beams from the K500 superconducting cyclotron at Michigan State University. The isotopic enrichments of the 1.0 mg/cm^2 thick ^{90}Zr and 3.0 mg/cm^2 thick ^{208}Pb targets were 98.5 and 99.9%, respectively. The reaction products were analyzed with the S320 broad range magnetic spectrograph and detected by the standard focal plane detector system (two resistive wire position counters, two ionization chambers, and a plastic scintillator), which ensured unambiguous particle discrimination. A thin film start detector placed near the exit to the scattering chamber was used together with the plastic scintillator to obtain the time of flight of ions through the spectrograph. The calibration of the focal

plane was determined independently for each incident energy and each target nucleus by measuring the position of the elastic peak along the counter for different magnetic fields. In order to check the differential linearity of the detection system, two different settings of the magnetic field were used at each energy, giving a shift of about 1% in the energy spectra. The overall energy resolution $\Delta E/E$ measured for the elastic peak varied from about 2×10^{-3} to 4×10^{-3} depending on its position along the focal plane.

During the experiment the elastic scattering counts were suppressed by masking a small part of the detection system with a 5 mm wide metal finger, which was located about one-third of the way down the focal plane. Under these conditions ^{19}Ne, ^{21}Ne, and ^{21}Na spectra could be accumulated together with inelastic data at the same magnetic field exposure although the mask did interfere slightly with some of the spectra.

The angular opening of the spectrometer was 1.5°. The ^{20}Ne+^{90}Zr system was studied at 5.3°, 7°, and 8° at 600 MeV and 6.4° at 500 MeV. With the ^{208}Pb target, spectra were accumulated at 7°, 9.5°, 11°, 13°, and 15° at 600 MeV incident energy, and at 11.5° at 500 MeV. Spectra obtained near the grazing angle for both target nuclei at both incident energies are displayed in Figs. 1 and 2. They have been linearized with respect to the center-of-mass kinetic energy loss (labeled E^* in the spectra) which is directly related to the sum of excitation energies of the final nuclei in the case of a two-body reaction. The accuracy of the value of this summed excitation energy is estimated to be better than 1 MeV.

The qualitative features of these spectra can be summarized as follows.

(i) The ^{21}Na spectra display a peak at low excitation energy (near 1 and 1.75 MeV for the ^{208}Pb and ^{90}Zr target nuclei, respectively) and a slowly decreasing tail extending from 4 to about 20 MeV. The Zr spectra also show a small maximum near 7 MeV. The full width at half maximum (FWHM) of the low energy peak at 500 MeV (600 MeV) is about 2.7 MeV (3.2 MeV) in ^{207}Tl and 2.2 MeV (2.5 MeV) in ^{89}Y.

(ii) Two peaks are observed in the ^{21}Ne spectra. They are located at about 2.5 and 6.5 MeV in ^{207}Pb and 0.5 and 6.25 MeV in ^{89}Zr. The FWHM of the higher energy bumps is about 3.5 MeV. However, there appears to be some internal structure in the low excitation energy peaks, especially at 500 MeV incident energy where slightly better resolution was obtained. Above 10 MeV, the cross section decreases slowly with summed excitation energy. (There is no information about the ^{21}Ne spectra above 15 MeV, because of the presence of the mask which intercepted the elastic peak.)

(iii) The ^{209}Pb(^{20}Ne,^{19}Ne) spectra at 500 and 600 MeV exhibit the following structures: a peak located at 1.5 MeV, a dip at 4 MeV, a second maximum at about 10 MeV and a falloff toward high excitation energies, with a weak shoulder at about 20 MeV. The ^{90}Zr(^{20}Ne,^{19}Ne) spectra have rather similar structures: a peak centered at about 2.5 MeV with a shoulder on its low energy side, a plateau from 7 to 10 MeV, and a second maximum at about 14 MeV. The high excitation energy part of the ^{19}Ne spectra may be explained by the existence of at least one strong resonancelike structure with a width of a few MeV (at about 10 MeV in ^{209}Pb and 14 MeV in ^{91}Zr, re-

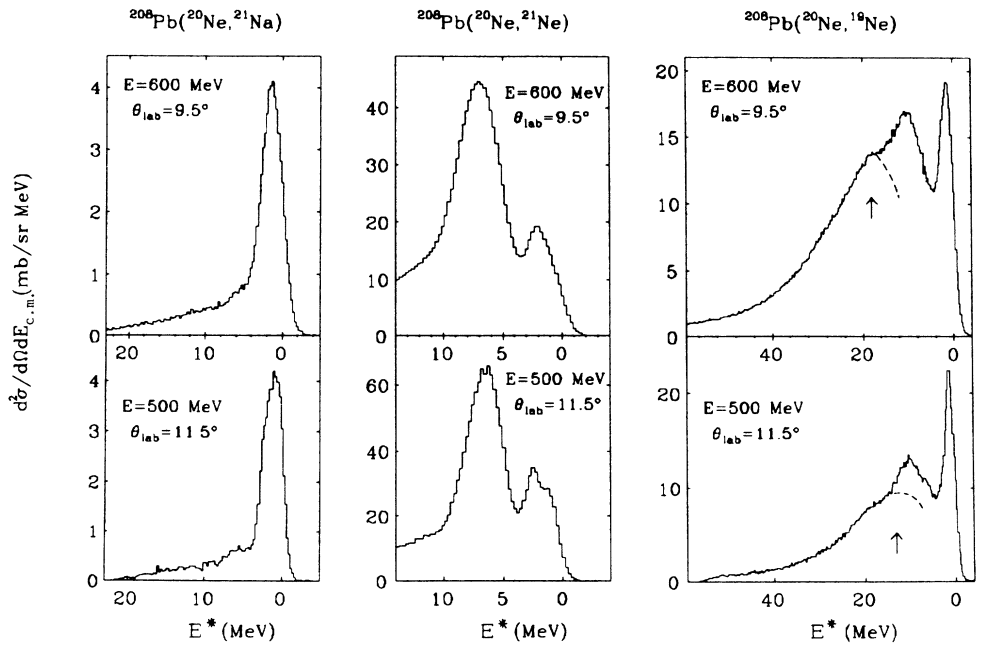

FIG. 1. Experimental spectra from the ^{20}Ne+^{208}Pb reactions at 500 and 600 MeV. The arrow indicates the position of ^{19}Ne ions moving with the beam velocity. The shape of the low excitation energy side of the breakup bump in the ^{19}Ne spectra is suggested by dashed lines. The dotted line in the 600 MeV spectrum indicates the linear background assumed in the estimation of the cross section of the 10 MeV bump (see text).

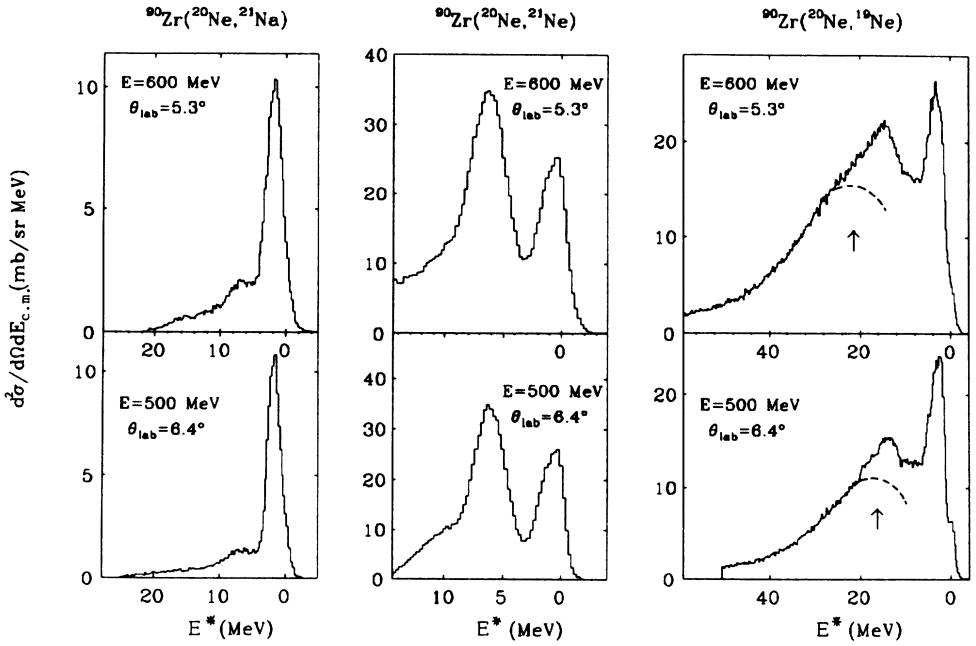

FIG. 2. Experimental spectra from the ^{20}Ne+^{90}Zr reactions at 500 and 600 MeV. The arrow indicates the position of the ^{19}Ne ions moving with the beam velocity. The shape of the low excitation energy side of the breakup bump in the ^{19}Ne spectra is suggested by dashed lines.

TABLE I. Spectroscopic data[a] used in the calculation of "theoretical" transfer spectra.

	E	nlj	C^2s		E	nlj	C^2S		E	nlj	C^2S
^{19}Ne[b]	0.00	$2s_{1/2}$	0.12	^{91}Zr[c]	0.00	$2d_{5/2}$	0.98	^{209}Pb[d]	0.00	$2g_{9/2}$	0.69
	0.24	$1d_{5/2}$	1.04		1.20	$3s_{1/2}$	0.93		0.78	$1i_{11/2}$	0.98
	0.27	$1p_{1/2}$	1.96		2.03	$2d_{3/2}$	0.45		1.42	$1j_{15/2}$	0.59
	1.53	$1d_{3/2}$	0.73		2.16	$1h_{11/2}$	0.41		2.49	$2g_{7/2}$	0.93
					2.19	$1g_{7/2}$	0.68				
					3.47*	$1g_{7/2}$	0.42				
					4.05*	$1h_{11/2}$	0.20				
		(S_p=6.41)				(S_n=7.19)				(S_n=3.94)	
^{21}Ne[e]	0.35	$1d_{5/2}$	0.62	^{89}Zr[f]	0.00	$1g_{9/2}$	8.00	^{207}Pb[b]	0.00	$3p_{1/2}$	2.00
	2.80	$2s_{1/2}$	0.80		0.59	$2p_{1/2}$	1.70		0.57	$2f_{5/2}$	6.20
	4.73*	$2p_{3/2}$	0.57		1.10	$2p_{3/2}$	2.48		0.90	$3p_{3/2}$	4.00
	5.33	($1f_{7/2}$	0.35)		1.64*	$1f_{5/2}$	3.50		1.63	$1i_{13/2}$	12.0
	6.16*	$1d_{3/2}$	0.46		(7.0)	$1f_{7/2}$	(8.0)		2.33	$2f_{7/2}$	7.30
									3.41	$1h_{9/2}$	6.90
		(S_n=6.71)				(S_p=7.86)				(S_n=6.74)	
^{21}Na[e]	0.33	$1d_{5/2}$	0.33	^{89}Y[h]	0.00	$2p_{1/2}$	1.80	^{207}Tl[g]	0.00	$3s_{1/2}$	1.90
	2.42	$2s_{1/2}$	0.22		0.91	$1g_{9/2}$	1.25		0.35	$2d_{3/2}$	3.40
					1.51	$2p_{3/2}$	3.90		1.35	$1h_{11/2}$	12.1
					1.75	$1f_{5/2}$	6.00		1.67	$2d_{5/2}$	4.20
					(7.0)	$1f_{7/2}$	(8.0)		3.48	$1g_{7/2}$	1.60
									(9.0)	$1g_{9/2}$	(10.)
		(S_p=2.43)				(S_p=7.07)				(S_n=6.84)	

[a]Only the strongest one-particle (or one-hole) bound states have been considered. Their excitation energies are given in MeV. Centroid energies of several levels are labeled with an asterisk. When exceeding the corresponding shell-model sum-rule limit, the C^2S values have been assumed equal to this limit. Here the $1f_{7/2}$ deep hole strengths in ^{89}Zr and ^{89}Y have been assumed to be concentrated around 7 MeV. S_n and S_p are the separation thresholds for neutron and proton, respectively.

[b]Reference 8.

[c]Reference 9.

[d]Reference 10.

[e]Reference 11. The C^2S value assumed for the 5.33 MeV level in ^{21}Ne is that used to calculate the spectra shown in Fig. 4 (see text).

[f]Reference 12.

[g]Reference 13.

[h]Reference 14.

spectively) superimposed on a much wider asymmetric structure some tens of MeV wide. The origin of these structures is discussed in Sec. IV.

III. COMPARISON WITH DWBA PREDICTIONS

Spectroscopic data about the main single-particle bound states in ^{21}Ne and ^{21}Na and single-hole states in ^{19}Ne are presented in Table I together with those in the corresponding final heavy nuclei. Apart from the contribution of three-body reactions, the spectra of Figs. 1 and 2 are expected to result from the addition of the various experimentally unresolved mutual excitations of the final nuclei. The shapes observed for these spectra suggest that some combinations of configurations are especially favored in the present transfer reactions. In order to test this interpretation, DWBA calculations were performed to study the selectivity of the ^{20}Ne induced transfer reactions at 500 and 600 MeV. Recent high-resolution studies of one-nucleon-transfer reactions induced by ^{12}C and ^{16}O of a few hundred MeV (Refs. 3–5) have shown that the relative cross sections for the excitation of different configurations could be well reproduced by DWBA calculations.

The DWBA calculations were performed with the full recoil finite range program PTOLEMY[6]. In the absence of elastic scattering data for all the systems under study, the same optical-model potential[7] was adopted for the interaction of ^{20}Ne with ^{90}Zr and ^{208}Pb at both incident energies. The parameters of the real and imaginary Woods-Saxon wells were $V=50$ MeV, $W=80$ MeV, $r_r=1.16$ fm, $r_i=1.13$ fm, $a_r=0.67$ fm, $a_i=0.5$ fm, reproducing data from elastic scattering of ^{20}Ne on ^{208}Pb at 600 MeV.[7] The same parameters were also used for the exit channels. The Woods-Saxon potential used to generate the bound states for the light ($A\sim20$) systems had a diffuseness of 0.65 fm, a reduced radius of 1.20 fm, and a spin-orbit potential strength $V_{SO}=7$ MeV.[4] The corresponding parameters for the heavy systems ($A\sim90$ and ~208) were taken equal to the values generally adopted in the analysis of transfer induced by light ions, i.e., $r=1.25$ fm, $a=0.65$ fm and $V_{SO}=6$ MeV.

The following procedure was adopted in order to compare the results of DWBA calculations to the data since individual levels in the light and heavy final nuclei could not be resolved experimentally. Theoretical spectra for each reaction at a particular angle and incident energy were first deduced from the DWBA cross sections weighted by the spectroscopic factors of the main single-particle and single-hole states in the final nuclei[8–14] as given in Table I. These theoretical spectra were then convoluted with a Gaussian shape (simulating the experimental energy resolution) and multiplied by a normalization factor in order to compare with experimental results. The full width at half-height of the Gaussian and the normalization factor were both adjusted in order to fit the low excitation energy part of the experimental spectra, where uncertainties about the distribution of spectroscopic strengths are smaller. The widths of the Gaussian peaks deduced from this analysis are given in the figure captions and were found to be consistent with the measured energy resolution of between 1 and 2 MeV reported above.

Both the experimental and the convoluted theoretical ^{21}Na, ^{21}Ne, and ^{19}Ne spectra at 500 MeV incident energy are displayed in Figs. 3–5. The positions and predicted strengths of the states are marked as vertical lines in the figures. The results of this analysis are discussed below.

A. Absolute cross sections

The results of the present DWBA calculations have been normalized to the data as described earlier. Any

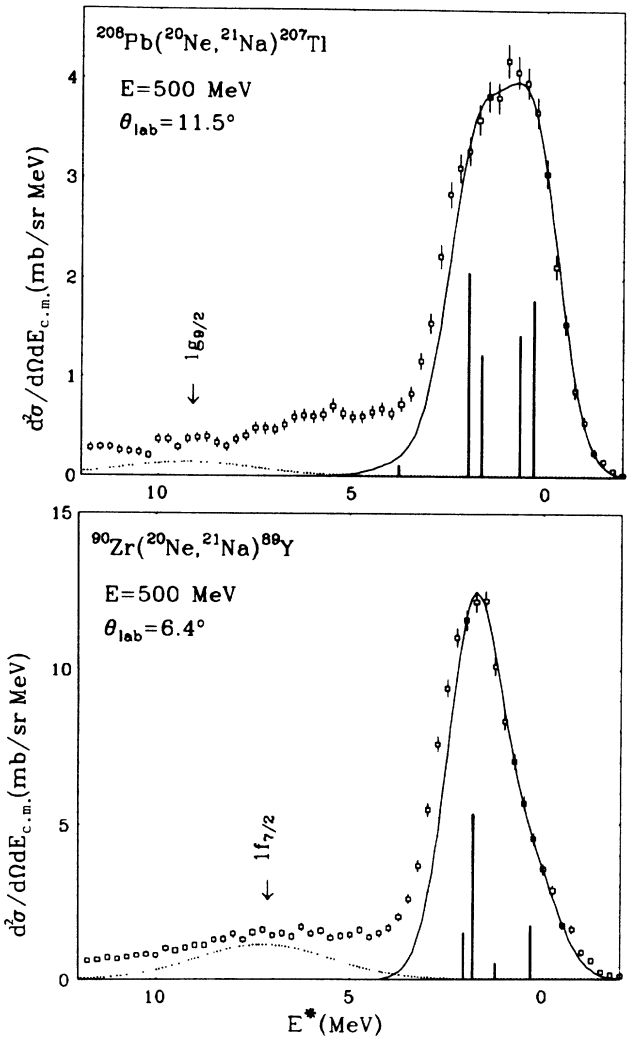

FIG. 3. Comparison between experimental ^{21}Na spectra (points with error bars) and calculated ones (full line) using a resolution parameter of 1.6 MeV. (The normalization factors were 1.80 and 1.18 for ^{89}Y and ^{207}Tl, respectively.) The DWBA predicted contributions of various combinations of configurations in ejectile and residual nuclei are represented by the length of vertical bars. Each vertical bar corresponds to a specific combination of configurations whose quantum numbers and excitation energies are given in Table I. The dotted lines at high excitation energy represent the calculated contribution of pickup from the internal $1f_{7/2}$ and $1g_{9/2}$ subshells in ^{89}Y and ^{207}Tl, respectively (see text).

large deviation of the normalization factor from unity would bring into question the validity of the DWBA method or at least cast doubts on the ingredients of the calculations such as optical potentials, form factors, and spectroscopic factors. The normalization factors extracted for the various reactions and reported in the figure captions were found to vary from 0.6 to 1.2 and 1.1 to 1.8 for the lead and zirconium targets, respectively. The corresponding normalization factors extracted at 600 MeV incident energy vary from 0.7 to 1.3 for lead and 1.0 to 1.9 for zirconium. Such a dispersion of the normalization factors seem quite reasonable considering the very crude assumptions made in the present DWBA calculations viz. using the same set of optical parameters for all the different channels. In the following, only the relative values of the theoretical cross sections will be discussed.

B. Angular distributions

Theoretical angular distributions calculated for one-nucleon transfer on ^{208}Pb for various $J_i \rightarrow J_f$ transitions display similar patterns with maxima near the grazing angle. The situation is slightly different for the ^{90}Zr target, as the angular distributions at small angles are pre-

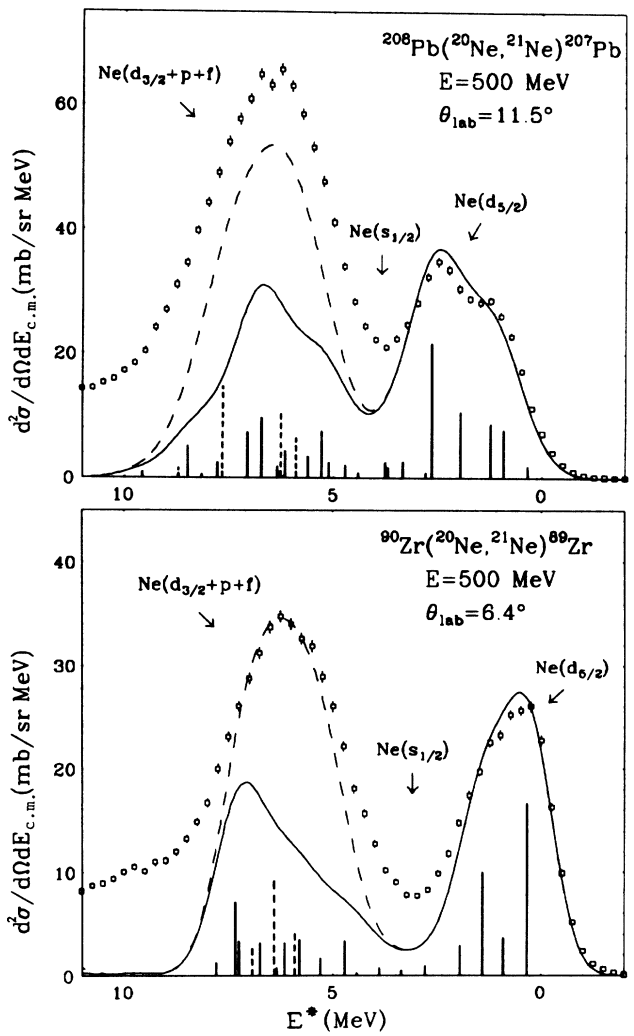

FIG. 4. Comparison between experimental ^{21}Ne spectra (points with error bars) and calculated ones (full line) using a resolution parameter of 1.3 MeV. (The normalization factors were 1.10 and 0.61 for ^{89}Zr and ^{207}Pb, respectively.) The DWBA predicted contributions of various combinations of configurations in ejectile and residual nuclei are represented by the length of vertical bars. Each vertical bar corresponds to a specific combination of configurations whose quantum numbers and excitation energies are given in Table I. The dashed lines represent the theoretical spectra calculated with an additional $1f_{7/2}$ excitation at 5.33 MeV in ^{21}Ne

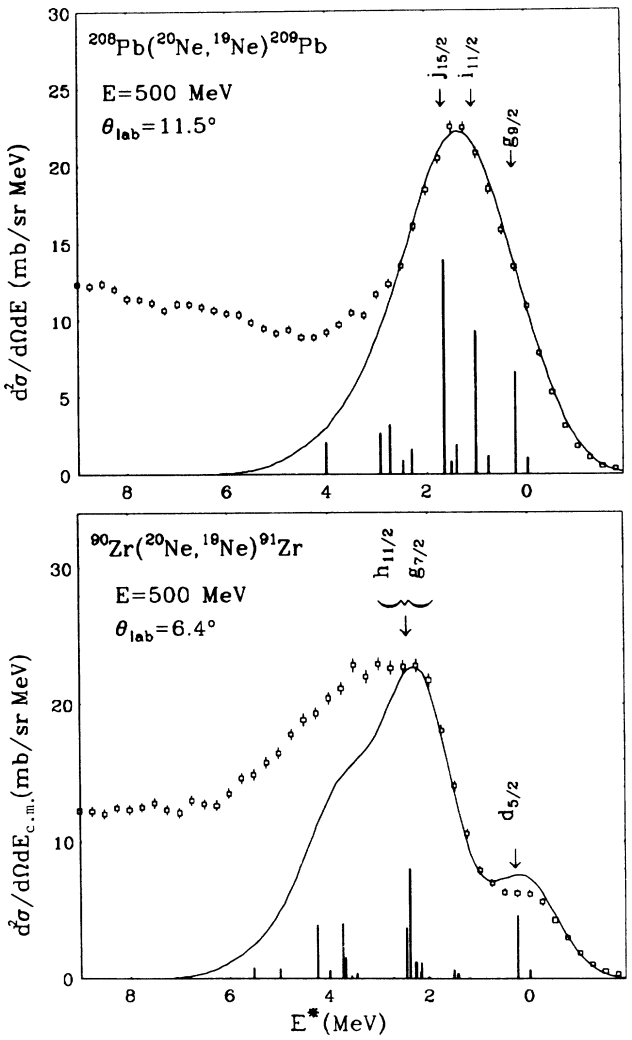

FIG. 5. Comparison between experimental ^{19}Ne spectra (points with error bars) and calculated ones (full line) using a resolution parameter of 1.5 and 1.8 MeV for ^{89}Zr and ^{209}Pb, respectively. The corresponding normalization factors were 1.60 and 1.02. The DWBA predicted contributions of various combinations of configurations in ejectile and residual nuclei are represented by the length of vertical bars. Each vertical bar corresponds to a specific combination of configurations whose quantum numbers and excitation energies are given in Table I. (Here the contributions of $p_{1/2}$ and $d_{5/2}$ ejectile excitations have been summed.)

dicted to be more dependent on the type of transition involved.

Experimental angular distributions measured for the bump at low excitation energy in the (^{20}Ne,^{19}Ne), (^{20}Ne,^{21}Ne) and (^{20}Ne,^{21}Na) reactions at 600 MeV are displayed in Fig. 6 with the predictions. These theoretical differential cross sections were obtained from the weighted sum of the contributions of the states reported in Table I, with a final normalization to the data. There is good agreement between the experimental angular distributions and the DWBA predictions over the observed angular range.

C. Energy distributions

1. The (^{20}Ne,^{21}Na) reaction

According to the DWBA calculations, there is only one bound single-particle state in ^{21}Na which contributes to the transfer cross sections, viz. the $1d_{5/2}$ level at 0.33 MeV. The contribution of the $2s_{1/2}$ state at 2.42 MeV is, in fact, predicted to be very small. The $3/2^+$ ground state and the $7/2^+$ state at 1.72 MeV are known not to be excited in one-nucleon-transfer reactions due to their collective nature.[11] Excitation of the ^{21}Na nucleus above the 2.43 MeV threshold energy for proton emission would contribute to the transfer-evaporation bump which dominates the ^{20}Ne inelastic spectra[2] at high excitation energies. The experimental shapes of the bumps in the ^{21}Na+^{89}Y ad ^{21}Na+^{207}Tl spectra are qualitatively well reproduced by DWBA calculations and assuming an experimental resolution of 1.6 MeV, as shown in Fig. 3. The ^{89}Y spectrum is consistent with a strong excitation of the $2p_{3/2}$ state at 1.51 MeV in ^{89}Y, as predicted by the DWBA, whereas the $3s_{1/2}$, $2d_{3/2}$, $1h_{11/2}$, and $2d_{5/2}$ single-proton-hole states below 1.7 MeV in ^{207}Tl are predicted to contribute almost equally to the cross section, giving rise to a broader low-lying peak is observed experimentally.

The excitation of deep hole states could be responsible for the high energy tail observed in the pickup spectra of Fig. 3. In particular, the $1f_{7/2}$ proton-hole strength in ^{89}Y has been located at about 7 MeV in both (e,e',p) and $(d,^3\mathrm{He})$ reactions[1] as a few MeV wide structure. The DWBA prediction for the excitation of the $1f_{7/2}$ hole state is shown in Fig. 3 (a Gaussian shape with a 4 MeV width at half maximum has been assumed here). It accounts for a large part of the cross section measured between 4 and 12 MeV in the ^{90}Zr(^{20}Ne,^{21}Na)^{89}Y spectrum. In a similar way, proton pickup in the internal subshells could be responsible for the high energy tail observed in the ^{208}Pb(^{20}Ne,^{21}Na)^{207}Tl spectrum. From previous $(d,^3\mathrm{He})$ results[1] the centroid of the $1g_{9/2}$ proton-hole strength in ^{207}Tl is located at about 9 MeV. The calculated contribution of this state in the (^{20}Ne,^{21}Na) reaction is shown as a dotted line in Fig. 3.

2. The (^{20}Ne,^{21}Ne) reaction

The doubled-peaked shape of the (^{20}Ne,^{21}Ne) spectra (cf. Fig. 4) is qualitatively well accounted for by DWBA calculations which include ejectile excitations. In fact, the calculations predict a much weaker cross section for the excitation of the $2s_{1/2}$ state at 2.80 MeV in ^{21}Ne than for the 0.35 MeV $1d_{5/2}$ state and the higher-lying known $1d_{3/2}$ and $2p_{3/2}$ states. This gives rise to a minimum at a

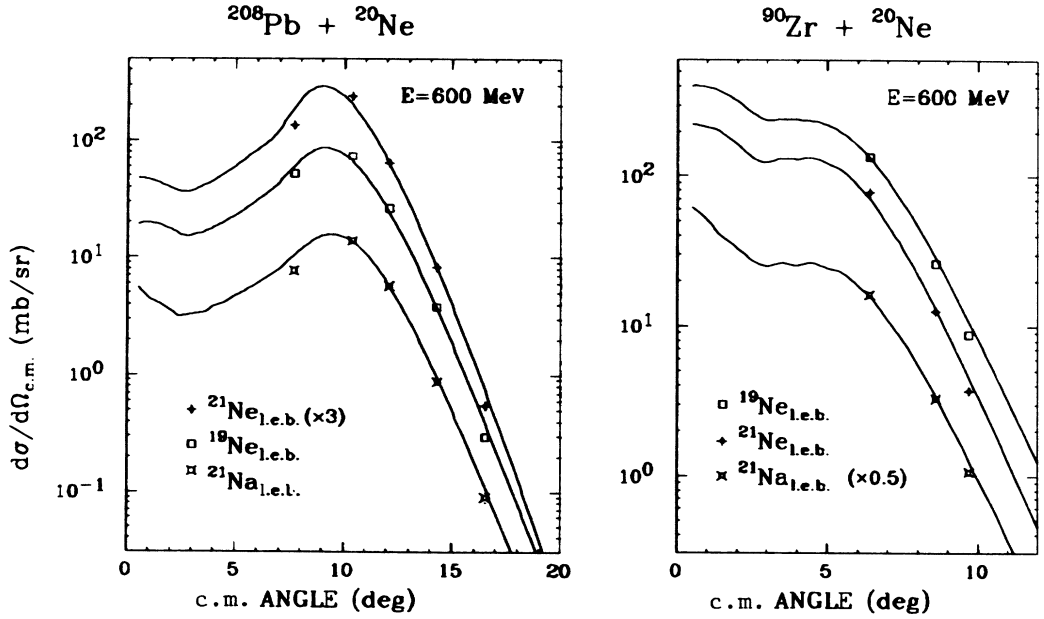

FIG. 6. Experimental angular distributions measured in the study of the ^{208}Pb+^{20}Ne and ^{90}Zr+^{29}Ne system at 600 MeV for the low energy bump (leb) observed in the ^{19}Ne, ^{21}Ne, and ^{21}Na spectra. The data points for ^{209}Pb+^{21}Ne and ^{89}Y+^{21}Na are presented multiplied by 3 and 0.5, respectively. The full lines are theoretical angular distributions (see text) normalized to the data.

summed excitation energy of about 3.5 and 4.5 MeV in the spectra of ^{89}Zr and ^{207}Pb, respectively. The strong excitation of the $1g_{9/2}$ ^{89}Zr ground state and of the $2f_{7/2}$ state at 2.33 MeV in ^{207}Pb, which is predicted by DWBA calculations, appears to be responsible for the difference between the shapes of the low energy bumps observed in Fig. 4 for the two residual nuclei.

From (d,p) studies at low incident energy it is known that about half of the $1d_{3/2}$ and $2p_{3/2}$ shell-model neutron strength in ^{21}Ne is located below the neutron threshold (cf. Table I). Under the assumption that only these ejectile excitations contribute, the present calculations can account for about one-third of the total cross section observed in the high energy bumps in both the ^{90}Zr(^{20}Ne,^{21}Ne) and ^{208}Pb(^{20}Ne,^{21}Ne) spectra (cf. Fig. 4). However, a large cross section for transfer to the $1f_{7/2}$ orbital is predicted by the DWBA calculations. There is no information about the location of the $1f_{7/2}$ neutron strength in ^{21}Ne, due to the small cross section expected for $l=3$ transfers in the low energy (d,p) reaction.[11] Excitation of $1f_{7/2}$ states above the neutron threshold would contribute to the transfer-evaporation bump observed in the ^{20}Ne inelastic spectra.[2] The contribution of so far unknown $1f_{7/2}$ bound levels on the (^{20}Ne,^{21}Ne) cross section was evaluated by assuming a $1f_{7/2}$ configuration for the 5.33 MeV level (previously proposed[11] to have a possible J^{π} value of $5/2^+$ or $7/2^-$). A significant part of the cross section around 6.5 MeV could be due to the mutual excitation of the 5.33 MeV level and single-hole states at low excitation energy in the residual nuclei, as is shown in Fig. 4, where the dashed lines correspond to an assumed $1f_{7/2}$ spectroscopic factor of 0.25. It is clear therefore, that the predominance of ejectile excitation in the (^{20}Ne,^{21}Ne) reaction makes the investigation of high-lying hole states in the residual nuclei in the 4–10 MeV excitation energy region difficult. Examples of such strength are the $1h_{11/2}$ bole strength at about 8 MeV in ^{207}Pb and the $1f_{7/2}$ hole strength at about 7 MeV in ^{89}Zr observed in light-ion pickup reactions.[1]

3. *The (^{20}Ne,^{19}Ne) reaction*

The most striking feature of this reaction suggested by the present DWBA calculations is the preferential excitation of high spin single-particle states in the residual heavy nucleus. The low energy part of the ^{19}Ne spectra is predicted to be dominated by transfers to the available high spin valence orbitals, namely the $1i_{11/2}$ and $1j_{15/2}$ subshells in ^{209}Pb and the $1g_{7/2}$ and $1h_{11/2}$ states in ^{91}Zr. It is also predicted that the ^{19}Ne ejectile is predominantly excited in the $1d_{5/2}$ and $1p_{1/2}$ neutron-hole states at 0.24 and 0.27 MeV, due to the small spectroscopic factor of the $2s_{1/2}$ ground state. The low energy parts of the experimental ^{19}Ne spectra are in fair agreement with the DWBA predictions, as shown in Fig. 5. According to the calculations, the bump experimentally observed at about 2.5 MeV in the ^{91}Zr spectra results mainly from the excitation of the $11/2^-$ and $7/2^+$ states at 2.16 and 2.19 MeV, whereas the main components of the 1.5 MeV bump in ^{209}Pb are the $11/2^+$ state at 0.78 MeV, the $15/2^-$ state at 1.42 MeV, and to a lesser extent, the $9/2^+$ ground state.

Such a selectivity for transfer to high spin single-particle states, which is generally encountered in stripping reactions at high incident energy, is due to the large mismatch between the initial and final grazing angular momentum values which favors the transfer of high angular momenta. Recent studies[3–5,10] of the $(\alpha,{}^3\text{He})$, (^{12}C,^{11}C), and (^{16}O,^{15}O) reactions at incident energies per nucleon of 45.7 , 40, and 49.5 MeV, respectively, have shown selective excitation of high spin neutron states in ^{209}Pb, which has been well reproduced by DWBA calculations.

The neutron emission thresholds in ^{209}Pb and ^{91}Zr are located at 3.9 and 7.2 MeV, respectively. It is not possible to calculate transfer to higher-lying unbound states with the available EFR-DWBA codes. Therefore, the structures observed at 10 MeV in ^{209}Pb and 14 MeV in ^{91}Zr can only be interpreted using general arguments about the selectivity of this reaction and also by comparing with the results of other stripping reactions such as $(\alpha,{}^3\text{He})$ and (^{12}C,^{11}C), as described in the next section.

IV. STRUCTURES AT HIGH EXCITATION ENERGY IN THE (^{29}Ne,^{19}Ne) REACTIONS

Various three-body reactions can be expected to contribute to the high-lying part of the ^{19}Ne spectra. Structures originating from a three-body contribution should be observed at apparent excitation energies which move with incident energy according to the kinematics of the reaction. The position of the bumps observed at 10 and 14 MeV summed excitation energy in the ^{208}Pb(^{20}Ne,^{19}Ne)^{209}Pb and ^{90}Zr(^{20}Ne,^{19}Ne)^{91}Zr reactions, respectively, is independent of incident energy. This suggests that these structures result from a neutron transfer to an unbound state in the residual heavy nucleus.

The determination of the excitation cross sections for high-lying states strongly depends upon the three-body background which is subtracted. An estimation of the cross section for exciting the 10 MeV state in ^{209}Pb has been made by arbitrarily subtracting a linear background between 6 and 16 MeV. The resulting angular distribution at 600 MeV incident energy is displayed in Fig. 7. Its shape is very similar to the angular distribution measured for the low energy bump in ^{209}Pb which is well reproduced by DWBA calculations. Angular distributions measured with the lead target for different energy slices of the ^{19}Ne spectrum are also shown in Fig. 7. They are observed to monotonically decrease with angle above 10°. Similar results have been obtained with the zirconium target.

We cannot exclude the possibility that some weak structures observed in the spectra (such as the shoulder at about 20 MeV in ^{209}Pb) correspond to the excitation of higher-lying states in the residual heavy nucleus. However, no clear evidence can be obtained from the present data as long as the exact shape of the underlying three-body background is not known. Any further detailed investigation of the high-lying structures observed in stripping spectra should correctly take into account the con-

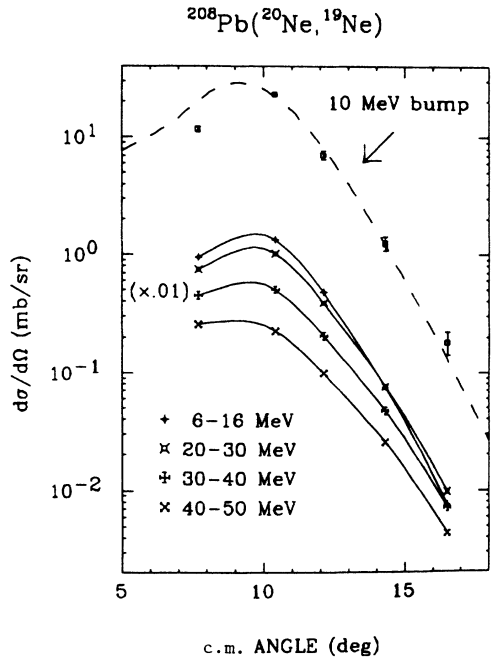

FIG. 7. Experimental angular distributions measured for the bump at 10 MeV and for various energy bins of the continuum in the ^{208}Pb(^{20}Ne,^{19}Ne) reaction at 600 MeV. The lines are to guide the eye.

tribution to the cross section of various three-body processes which are expected to occur above the particle emission thresholds. However, it can be noticed that elastic breakup of the incident ^{20}Ne projectile in the Coulomb field of the target nucleus into ^{19}Ne plus one neutron could be responsible for at least part of the large bump observed at high excitation energies in the (^{20}Ne,^{19}Ne) spectra of Figs. 1 and 2. In such a case, the average energy of the outcoming ^{19}Ne is expected to correspond to a velocity equal to that of the incident beam. The central position expected for this breakup bump is indicated with an arrow in Figs. 1 and 2. The qualitative agreement of these theoretical positions with the general behavior of the spectra for both target nuclei and both incident energies supports this simple interpretation.

High-lying structures in stripping spectra were first observed in a study[1] of the (α,^{3}He) reaction at 183 MeV. In particular, a bump located at about 10.5 MeV in ^{209}Pb similar to that observed in Fig. 1 has been reported in Ref. 10. Using arguments based on theoretical predictions about the location of outer subshells and results of a DWBA analysis, it has been proposed[1,4] that the 10.5 MeV bump in ^{209}Pb arises from the excitation of one neutron in external high spin subshells, particularly the $1k_{17/2}$ orbital. In a similar way the bump observed in the (α,^{3}He) reaction at 14 MeV in ^{91}Zr has been proposed[1] to arise from the excitation of the $1i_{3/2}$ orbital. It seems probable that the high-lying bumps in ^{209}Pb and ^{91}Zr observed in the (^{20}Ne,^{19}Ne) reaction at 25 and 30 MeV/nucleon have the same origin.

In addition to the (α,^{3}He) results, there have been recent investigations of the high excitation energy region of ^{209}Pb by several heavy-ion-induced stripping reactions[3,4,15] with different selectivity. The assumption that the 10 MeV structure in ^{209}Pb mostly originates from a neutron transfer in the external $1k_{17/2}$ orbital is supported by the observation of a similar peak in the (^{12}C,^{11}C) reaction at 40 MeV/nucleon (Ref. 4) where transfer to high spin orbitals with $J = l + \frac{1}{2}$ is favored.

One may note that the excitation energy of the high-lying structures observed in ^{209}Pb (about 10 MeV) and in ^{91}Zr (about 14 MeV) is approximately equal to that of the giant quadrupole resonance (GQR) in the corresponding target nucleus, which has been shown to dominate the inelastic spectra.[2] However, the excitation of the GQR is expected to proceed mainly via two-step mechanisms due to its particle-hole structure. Therefore, the selectivity of the present reaction for transfer to high spin orbitals makes the probability for exciting the GQR rather unlikely, as compared to the possible direct excitation of high-lying high spin single-particle states.

V. CONCLUSION

The low excitation energy parts of the present one-nucleon-transfer spectra are qualitatively well reproduced by DWBA calculations. Ejectile excitations are clearly responsible for the major differences between the spectra observed in the proton and neutron pickup reactions: the high excitation energy bump in the (^{20}Ne,^{21}Ne) reaction is related to the mutual excitation of $1d3/2$, $1p3/2$, $1f7/2$ shell-model states in ^{21}Ne and neutron-hole states in the heavy nucleus, whereas the excitation of mirror states in the (^{20}Ne,^{19}Ne) transfer reaction is dominated by transfer to high spin, single-particle states in the heavy residual nucleus. Structures observed at high excitation energy in the ^{19}Ne spectra are interpreted as unbound single-particle states resulting from a neutron transfer in a high spin external orbital. Any further investigation to confirm the present conclusions and eventually to investigate other higher-lying single-particle states requires a more precise determination of the underlying three-body continuum or a strong reduction of this background through coincidence experiments.

ACKNOWLEDGMENTS

We would like to thank the operating crew of the National Superconducting Cyclotron Laboratory (NSCL) K500 cyclotron for the efficient running of the accelerator. We also acknowledge fruitful discussions with Dr. J. Barrette and Dr. D. Brink. This work was supported in part by the U.S. National Science Foundation.

*On leave from IPN Orsay, France. Present address: University of South Carolina, Columbia, SC 29208.

[1]S. Gales, Ch. Stoyanov, and A. I. Vdovin, Phys. Rep. **166**, 127 (1988), and references therein.

[2]S. Fortier, S. Gales, S. M. Austin, W. Benenson, G. M. Crawley, C. Djalali, J. H. Lee, J. Van der Plicht, and J. S. Winfield, Phys. Rev. C **36**, 1830 (1987).

[3]M. C. Mermaz *et al.*, Z. Phys. A **326**, 353 (1987).

[4]E. Tomasi-Gustaffson, Thèse de Doctorat d'Etat Universite Paris-Sud, 1988; M. C. Mermaz *et al.*, Phys. Rev. C **37**, 1942 (1988) and references therein.

[5]J. S. Winfield, E. Adamides, S. M. Austin, G. M. Crawley, M. F. Mohar, C. A. Ogilivie, B. Sherrill, M. Torres, G. Yoo, and A. Nadasen, Phys. Rev. C **39**, 1395 (1989).

[6]M. H. Macfarlane and S. C. Pieper, Argonne National Laboratory Report No. ANL-76-11, 1976.

[7]M. Buenerd, J. Chauvin, G. Duhamel, J. Y. Hostachy, D. Lebrun, P. Martin, P. O. Pellegrin, G. Perrin, and P. de Saintignon, Phys. Lett. **167B**, 379 (1986).

[8]F. Ajzenberg-Selove, Nucl. Phys. **A300**, 122 (1978).

[9]C. R. Bingham and M. L. Halbert, Phys. Rev. C **2**, 2297 (1970).

[10]C. P. Massolo, F. Azaiez, S. Gales, S. Fortier, E. Gerlic, J. Guillot, E. Hourani, and J. M. Maison, Phys. Rev. C **34**, 1256 (1986).

[11]P. M. Endt and C. Van der Leun, Nucl. Phys. **A214**, 1 (1973).

[12]S. Gales, E. Hourani, S. Fortier, H. Laurent, J. M. Maison, and J. P. Schapira, Nucl. Phys. **A288**, 221 (1977).

[13]M. R. Schmorak, Nucl. Data Sheets **43**, 383 (1984).

[14]A. Stuirbink *et al.*, Z. Phys. **297**, 307 (1980).

[15]M. A. G. Fernandes, F. E. Bertrand, R. L. Auble, R. O. Sayer, B. L. Burks, D. J. Horen, E. E. Gross, J. L. Blankenship, D. Shapira, and M. Beckerman, Phys. Rev. C **36**, 108 (1987).